Direct Convection Correction for Cylindrical Radiometer Measurement

by

Sai Susmitha Guddanti

A Thesis Presented in Partial Fulfillment
of the Requirements for the Degree
Master of Science

Approved April 2023 by the
Graduate Supervisory Committee:

Konrad Rykaczewski, Chair
Jennifer Vanos
Robert Wang
Richard Burke

ARIZONA STATE UNIVERSITY

May 2023

ABSTRACT

Human exposure to extreme heat is becoming more prevalent due to increasing urbanization and changing climate. In many extreme heat conditions, thermal radiation (from solar to emitted by the surrounding) is a significant contributor to heating the body, among other modes of heat transfer. Therefore, accurately measuring radiative heat flux on a human body is becoming increasingly important for calculating human thermal comfort and heat safety in extreme conditions. Most often, radiant heat exchange between the human body and surroundings is quantified using mean radiant temperature, T_{mrt}. This value is commonly measured using globe or cylindrical radiometers. It is based on radiation absorbed by the surface of the radiometer, which can be calculated using a surface energy balance involving both convection and emitted radiation at steady state. This convection must be accounted for and is accomplished using a traditional heat transfer coefficient correlation with measured wind speed. However, the utilized correlations are based on wind tunnel measurements and do not account for any turbulence present in the air. The latter can even double the heat transfer coefficient, so not accounting for it can introduce major errors in T_{mrt}.

This Thesis focuses on the development, and testing of a cost-effective heated cylinder to directly measure the convection heat transfer coefficient in field conditions, which can be used for accounting convection in measuring T_{mrt} using a cylindrical radiometer. An Aluminum cylinder of similar dimensions as that of a cylindrical radiometer was heated using strip heaters, and the surface temperature readings were recorded to estimate the convection heat transfer coefficient, h. Various tests were conducted to test this concept. It was observed that heated cylinders take significantly less

time to reach a steady state and respond to velocity change quicker than existing regular-sized globe thermometers. It was also shown that, for accurate estimation of h, it is required to measure the outer surface temperature than the center temperature. Furthermore, the value calculated matches well in range with classic correlations that include velocity, showing proof of concept.

DEDICATION

To all the young girls that dream of science. I did it, and so can you.

ACKNOWLEDGMENTS

Firstly, I want to express my immense gratitude towards Dr. Konrad Rykaczewski for providing me with invaluable advice, continuous support, and remarkable patience during the course of my Thesis. I would also like to extend my sincere appreciation to Dr. Jennifer Vanos, who has supported me throughout my research. Additionally, I would like to thank my committee members, Dr. Robert Wang, and Mr. Richard Burke, for their valuable time and insightful critiques, which have greatly enriched my academic research and personal growth. Furthermore, I am grateful to my team members and colleagues, Shri, Ankit, Daniel, Lyle, and Emily, for their generous assistance and unwavering support, making my research journey enjoyable and memorable. Last but not least, I want to express my heartfelt gratitude to my parents and close friends, who have been my pillars of strength, constantly motivating me to surpass my limitations. Without their unwavering support, completing my study would have been impossible.

TABLE OF CONTENTS

Page

LIST OF TABLES

Table Page

CHAPTER 1

INTRODUCTION AND OVERVIEW

1.1 Why is Radiative Heating of the Human Body Important?

All life forms since the dawn of life from a mere metal-clay clump craved food and shelter for warmth. The stories of people living in caves during early ages to protect themselves from extreme temperatures prove that the concept of seeking thermal comfort is not new to us. The advent of humankind and the need to live a better, more comfortable life brought out our curiosity to build the world we see today. The associated urbanization has been rapid, with about 56% of the world population living in urban areas [1], and is expected to continue [2], playing a significant role in trapping the heat and elevating city temperatures due to the heat island effect [3], [4]. With the increase in Earth's average air temperature, extreme heat events become more frequent and intense [5]. In other words, more people are living in cities, which are getting hotter for multiple reasons. As such, a quantitative understanding of how a human body interacts with extremely hot surroundings is becoming increasingly important. Such knowledge can help us make informed decisions on future designs of everyday objects that impact our thermal balance ranging from the built environment to clothing.

The human thermoregulatory system maintains a core temperature of about 37°C by regulating heat production within and dissipation from the body [6]. When the body is exposed to extreme temperatures, whether hot or cold, the ability of the body to regulate heat effectively through thermoregulation alone is very limited, causing severe health impacts and, in extreme cases, even death [7], [8].

In 1972, Fanger proposed a basic heat exchange approach to quantifying how weather conditions combined with the indoor or outdoor built environment and human factors (e.g., activity, clothing, behavior) impact our thermal safety and comfort. He identified six relevant factors [9]: (1) internal heat production per unit body, (2) the thermal properties of clothing, (3) the temperature of the air surrounding, (4) the mean radiant temperature, (5) the pressure of water vapor in ambient air, and (6) the relative air velocity. Combining these factors into a human heat load, which is the net heat flux in the body considering all the heat flowing in and out of the body, we obtain [10]:

$$S\ (W/m^2) = E + R + C + K - H = E + R + C + K - (M - W) \qquad (1.1)$$

Where S is the rate of heat storage in the body, H is the internal heat production by the body, M is the metabolic rate of the body, W is mechanical work done by the body, E is sweat evaporation, R is radiation, C is convection, and K is conduction [6] When the body's thermal balance with the surrounding is disrupted, heat is accumulated in or released from the body, changing the core temperature.

When the rate of heat storage is positive, the body gains more heat than it is losing to the surrounding, and therefore the body's core temperature rises. This imbalance can occur when the ambient temperature is high, when the body engages in physical activity that generates heat, or when there is an additional external heat source, such as solar radiation. On the other hand, when the rate of heat storage is negative, the body loses more heat than it gains, and therefore the body's core temperature falls. This can occur when the ambient temperature is low, when the metabolic heat generation is low, or when there is an external cooling source (e.g., Windchill, or a radiative cooling panel [11]). The signs of the rest of the terms on the right-hand side can be determined based on a similar approach,

depending on if the heat is transferred into or out of the body. The evaporative, convective, and radiative terms in Equation (1.1) can be further grouped into skin and respiratory terms:

$$Q_{sk} = C + R + E_{sk} \qquad Q_{res} = C_{res} + E_{res} \tag{1.2}$$

Where the total rate of heat loss from the skin is Q_{sk} and the total rate of heat loss through respiration is Q_{res}. Q_{sk} can be further broken down into the convective, radiative evaporative fluxes (i.e., as C, R, E_{sk}) and Q_{res} into convective and evaporative fluxes (C_{res} and E_{res}).

From Equation (1.2), we can see that radiation and convection play a role in heat balance and thermal load [10]. In some extreme conditions, radiation becomes the primary factor influencing thermal load, for example, when wind speeds are minimal in arid (i.e., low cloud coverage) and hot regions such as Arizona. The radiation comprises of multiple direct, reflected, or diffuse sources in the short-wave (i.e., solar) and long-wave (i.e., infrared) spectral regions [12]. To facilitate the interpretation of these complex heat sources, their cumulative heating effect is often simplified into a single "artificial" metric in terms of an equivalent temperature referred to as the mean radiant temperature, T_{mrt}. In typical indoor settings T_{mrt} is equal to the air temperature. However, in arid and hot climates such as Arizona, the values of T_{mrt} can be extreme. For example, Middel et al. observed that during peak time with the air temperature of 48.5°C, a building canyon oriented in the east-west direction on the ASU Tempe campus, featuring bright concrete and walls that receive direct sunlight had T_{mrt} of 76.4°C [2]. Thus, in this case, radiation was the dominant mechanism in the human heat load. Furthermore, in clothing-microclimate (between skin and clothing), 65 to 70% of heat exchange occurs through radiative heat transfer[13]. In summary, human exposure to extreme heat is on the rise, and

in many of the hottest conditions, radiation is a dominant way of heating the body. This knowledge gives us a strong reason to better understand radiative heat exchange between the human body and the surrounding environment. In the following subsections, we discuss in depth the definition of T_{mrt} and common ways to measure it.

1.2 Overview of Mean Radiant Temperature (T_{mrt})

Mean radiant temperature is defined as "the temperature of a uniform enclosure with which a small black sphere at the test point would have the same radiation exchange as it does with the real environment" [6]. In simpler terms, it is a metric of the total radiant heat exchange between the human body and the surrounding thermal environment [14]. Barker initially introduced this concept, which utilized the method of view factors to model the radiant heat exchange between a theoretical blackbody and its surroundings [15]. Using a single temperature value, this approach allows the estimation of the radiant heat exchange between a complex shape, such as the human body, and its environment.

If two surfaces are assumed to be perfect emitters ($\varepsilon_1 = \varepsilon_2 = 1$), the radiant heat exchange between them, Q_r (units of W/m^2), can be estimated using Equation (3).

$$Q_r = \sigma F_{1\to2}(T_1^4 - T_2^4) \tag{1.3}$$

Where σ is Stefan Boltzmann constant, $F_{1\to2}$ is the surface view factor, which can be defined as the amount of radiation leaving surface 1 and reaching surface 2, T_1 and T_2 are the temperatures of the two surfaces under consideration. In most cases, the human body's surrounding comprises many surfaces. The mean radiant temperature, T_{mrt}, can be approximated using Equation (4):

$$T_{mrt} = \Sigma_{i=1}^{n} T_i^4 F_{p\to i} \tag{1.4}$$

Where T_i and $F_{p\rightarrow i}$ are each surface's temperature and view factor, respectively [16]. Employing Equations 1.3 and 1.4, we can calculate the radiative flux between a person with an assumed uniform surface temperature T_p and their surrounding as:

$$Q_{person-surrounding} = \sigma\,(T_p^4 - T_{mrt}^4) \tag{1.5}$$

However, accounting for each surface view can become intractable with many surface view factors at play. In addition, most surfaces are not perfect emitters and reflectors, further complicating theoretical analysis. Such complexities in calculating the $Q_{person-surrounding}$ can be avoided with experimental measurement of T_{mrt}. In the next sub-section, we describe common experimental approaches to these measurements.

1.3 Overview of Common Approaches to Measuring T_{mrt}

Common approaches to measure T_{mrt} include net radiometers, globe thermometers, and cylindrical radiometers [14] (see Figure 1.1). The net radiometer provides direct measurements of radiative fluxes. Consequently, it is considered the most accurate approach to measuring T_{mrt}[17]. In particular, the instrument (see Figure 1.1a, MaRTy) simultaneously measures short-wave and long-wave radiation from six different directions using pyranometers and pyrgeometers. The T_{mrt} is subsequently calculated from the integral radiation measurement using weight angular factors for a human being [18], [19] and assumed average radiative properties as: [2]

$$T_{mrt} = \sqrt[4]{\left(\frac{\Sigma_{i=1}^{6} W_i(a_k K_i + a_l L_i)}{a_l \sigma}\right)} - 273 \tag{1.6}$$

Where W_i are angular weighting factors for standing reference person for radiation incident from direction i (0.06 for up and down facing sensors and 0.22 for cardinal

direction sensors), a_k are the absorption coefficients for short-wave radiation (0.7), a_k long-wave radiation (0.97), K_i are the short-wave radiant fluxes, L_i are long-wave radiant fluxes, and σ is Stefan-Boltzmann constant [2]. While providing detailed measurements, the devices like MaRTy can cost as much as $20,000 to $30,000, making them expensive for simultaneous multi-site measurements.

(a) (b) (c)

Figure 1.1. (a) MaRTy, (b) Standrad globe Thermometer, and (c) Tan color-coated CR

The standard globe thermometers and cylindrical radiometers are more cost-effective routes to measure T_{mrt}[20], but their accuracy is decreased by the need to account for convective contributions among other drawbacks. In the next sub-sections, we describe these instruments in more depth.

1.4 Review of Globe Thermometers

Using spheres to measure radiation and convection to indicate their effect on human thermal comfort has been in the picture since the 19th century [9]. Many versions paved the way for the globe thermometer, introduced by Vernon [10]. Such devices use a thermocouple or thermistor placed at the center of a globe to measure the effective temperature of the surroundings (see Figure 1.1b, the globe thermometer). In 1934 Bedford and Warner introduced correcting for convection to measure T_{mrt} and validated that using it along with an ordinary thermometer and silvered kata-thermometer would yield reliable results [11]. Since then, standard globe thermometers have become the most common method to measure T_{mrt} [12].

However, the standard globe thermometers are made of metal (e.g., Copper) with about 15 cm in diameter [21], [22] and take approximately 20 minutes to reach steady [23], making them unsuitable for outdoor conditions where the environmental conditions are volatile. This issue was addressed when acrylic globe thermometers, also called ping-pong globe thermometers, were introduced by de Dear in 1987 and are known to significantly speed up the time taken to reach a steady state [24], [25] The spherical shape, however, is only well-suited for indoor environments, where the radiation is typically isotropic [14].

Short-wave (e.g., direct solar beam) and long-wave radiation can be highly anisotropic in outdoor environments. Due to this directionality, the body posture strongly impacts exposure to, for example, direct solar radiation [26]. When a sphere is exposed to the sun, the radiation it absorbs does not vary with the changes in the sun's angle [27]. However, in the case of a cylinder, the amount of radiation absorbed at different sun's

angles closely matches that of most humans (albeit simplified to be axisymmetric [18], [19]). This is why spheres are a poor representation of humans, especially when measuring T_{mrt} in outdoor conditions. Instead, the cylindrical shape can better match the shape of humans; therefore, using a Cylindrical Radiometer (CR) can provide more realistic radiation measurements [17], [20], [28]. The following section will discuss traditional CR and potential routes for their improvement.

1.5 Review of Cylindrical Radiometer (CR)

According to Dufton's report in 1930, an instrument known as a Eupatheoscope was designed to measure the effective temperature of a room [14]. Effective temperature can be considered an earlier version of mean radiant temperature, defined as "the temperature of a uniform enclosure in which, in still air, a sizable blackbody at about 24℃ would lose heat at the same rate as in the environment." The device is a 55.8 cm tall and 19 cm diameter hollow copper cylinder coated with black paint. It is heated electrically, and the power input can be utilized to determine the heat transfer rate between the cylinder and its surroundings. Later in 1986, the term Cylindrical Radiation Thermometer or Cylindrical Radiometer (CR) was defined by Brown and Gillespie [29]. The device is an unheated cylinder with much smaller dimensions (e.g., 1 cm diameter and 11 cm height) that has a thermocouple placed at its center and is filled with a thermally conductive epoxy to secure it (see Figure 1.1c, CR). Several dimensions were considered over the years [20], [29]. The smaller size allows the CR to reach a steady state more quickly than a large Eupatheoscope.

1.6 Determination of T_{mrt} from Globe or Cylindrical Radiometer Measurements

Both the globe and cylindrical radiometers measure a temperature within their centers, which then is used in a surface energy balance at steady state to determine the T_{mrt} at steady state. As shown in Figure 1.2, the total radiation absorbed by the devices, R_{abs}, is equal to the sum of the radiation emitted by the thermometer surface, R_{em}, and the convective heat transfer of the surrounding with the surface, Q_{con}:

$$R_{abs} = R_{em} + Q_{con} \tag{1.7}$$

For an object with an average surface temperature, T_s, the Equation can be rewritten as:

$$R_{abs} = \varepsilon_1 \sigma (T_s + 273.15)^4 + h(T_s - T_a) \tag{1.8}$$

where T_a is the surrounding air temperature, and h is the average convective heat transfer coefficient. The T_s in both the globe thermometer and CR is assumed to be equal to the center temperature, which may only sometimes be the case [8]. The above Equation can be re-arranged to:

$$T_{mrt} = \sqrt[4]{\frac{R_{abs}}{\varepsilon_1 \sigma}} - 273.15 = \sqrt[4]{(T_s + 273.15)^4 + \frac{h}{\varepsilon_1 \sigma}(T_s - T_a)} - 273.15 \tag{1.9}$$

This Equation makes it evident that accurate determination of the heat transfer coefficient (h) is critical for T_{mrt} calculation. Traditionally, h is estimated based on velocity and Reynolds number using existing correlations for cylinders in crossflow [30], [31]. However, in prior CR studies, only correlations for flow without incoming turbulence were used (i.e., zero turbulence intensity, see Table 1.1). In contrast, the average turbulence intensity on a pedestrian level in outdoor settings is in the 20% to 50% range

[32]. As we discuss next, turbulence in the incoming air can even double the heat transfer coefficient, so neglecting it likely causes substantial errors in T_{mrt} calculation.

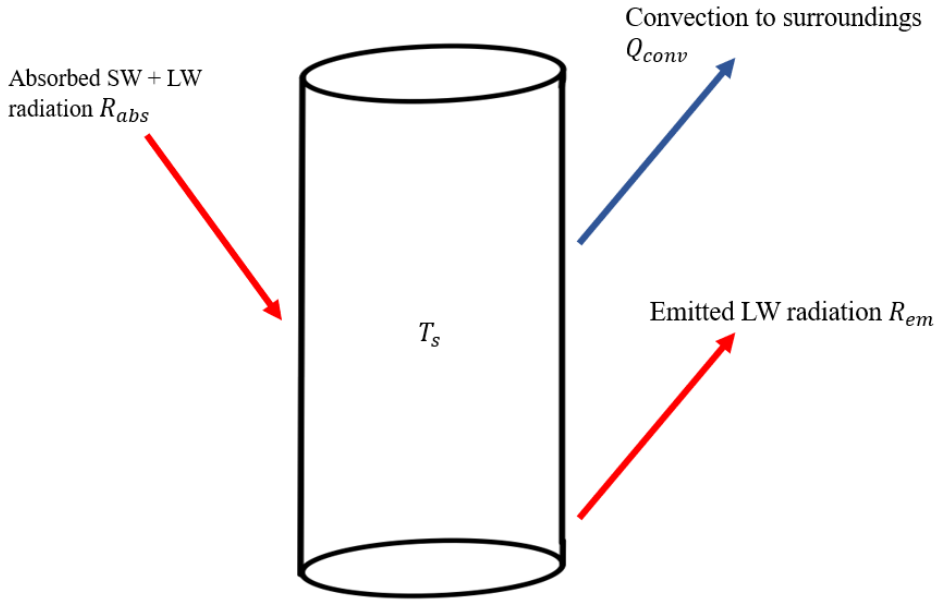

Figure 1.2. A surface energy balance on an unheated CR at steady state.

1.7 Motivation and Thesis Focus

If convective losses are appropriately accounted for, Cylindrical Radiometers could be a cost-effective and broadly representative way to measure T_{mrt}. Currently, the convective losses are estimated based on wind speed measurements input in classical heat transfer coefficient correlations that neglect turbulence intensity of the air (see the top of Table 1.1). There are several correlations in the literature that does account for such effects. See Table 1.1.

S.No	Name	Correlation	Range
1	Hilpert[30]	$Nu = A\, Re_D^m Pr^{1/3}$	Where A = 0.683; m=0.466 for $40 \le Re_D \le 4000$
2	Churchill & Berstein [31]	$Nu = \left(0.3 + \frac{0.62 Re_D^{\frac{1}{2}} Pr^{\frac{1}{3}}}{\left[1 + \left(\frac{0.4}{\mathrm{Pr}}\right)^{\frac{2}{3}}\right]^{\frac{1}{4}}} \left[1 + \left(\frac{Re_D}{282000}\right)^{\frac{5}{8}}\right]^{\frac{4}{5}} \right)$	Where Re_D Pr ≤ 0.2 ; $Re_D \le 10^7$; Pr = 0.7;
3	Kondjoyan & Daudin[33]	$Nu = \left(1.07 + 0.015\, TI\sqrt{Re}\right) 0.63\sqrt{Re}$	Pr = 0.7 ; 3000 < Re < 40,000; 1% < TI < 45%
4	Lowery & Vachon[34]	$Nu = 0.686\sqrt{Re} + 0.043\, TI\, Re$	Pr = 0.7 ; 109,000 < Re < 302,000; 0.4% < TI < 14.2%
5	Sikmanovic[35]	$Nu = 0.25\, Re^{0.618} + 0.488 Re^{1.118}\left(\frac{TI}{100}\right) - 0.914 Re^{1.618}\left(\frac{TI}{100}\right)^2$	Pr = 0.7 ; Re = 19,000; 2.5% < TI < 16%
6	J Ahn et al.[36]	$Nu = \left[629.4\left(\frac{TI}{100}\right)^2 + 20\left(\frac{TI}{100}\right) + 63.6\right] \cdot \left[-0.05\left(\frac{Re}{10000^2}\right) + 0.7\left(\frac{Re}{10000}\right) + 0.35\right]$	Pr = 0.7 ; 10,000 < Re < 50,000; 1% < TI < 10%
7	Mehendale et al.[37]	$Nu = 0.902\, Re + 2.14 Re\left(\frac{TI}{100}\right) - 2.89\sqrt{Re^3}\left(\frac{TI}{100}\right)^2$	Pr = 0.7 ; 25,000< Re < 100,000 0.73% < TI < 15.2%
8	Sak et al.[38]	$Nu = 0.78\sqrt{Re} - 3.49$	Pr = 0.7 ; 18,000< Re < 34,000 TI<0.6%
		$Nu = 114.2 + 465.9 TI$	Re = 27,000; 3% < TI < 8.2%

Table 1.1. Overview of existing correlations for heat transfer coefficient from a cylinder in crossflow that do and do not considers turbulence intensity (TI%) and Reynolds number (Re).

Using Kondjoyan & Daudin correlation, the plot in Figure 1.3 shows that varying the turbulence intensity from 6% to 40% can change a heat transfer coefficient by even an order of magnitude. However, none of these correlations were validated for the range of Re ($Re = \frac{V_a D}{\nu_{air}}$) of interest to CR. In particular, with a diameter of 1 cm and wind speed

of 0.25 to 4 m/s typical of hot and arid climate [39], the Re number range is about 100 to 2500, while the lowest validate range for any of the correlations is 3000. In addition, the experimental quantification of the turbulence intensity needed for these correlations requires a substantially more sophisticated (and expensive) high-speed anemometer than employed currently in most budget-oriented weather stations that might include a CR.

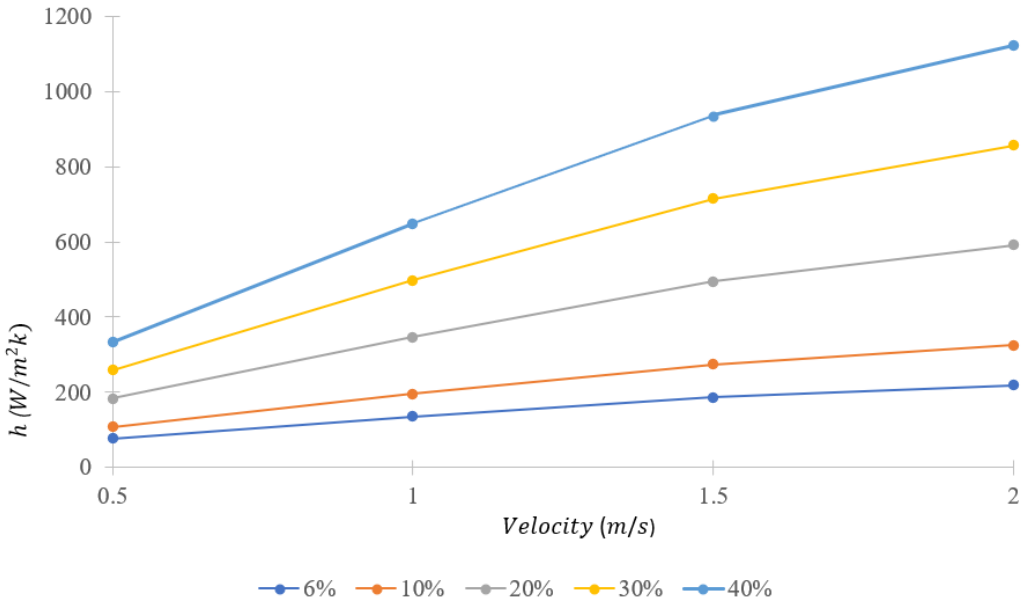

Figure 1.3. The convective heat transfer coefficient (h) calculated using Kondjoyan & Daudin correlation for a 0.95cm diameter cylinder as a function of air velocity for turbulence intensity of 6, 10, 20, 30, and 40%.

This Thesis focuses on the development of a cost-effective heated cylinder that can directly measure the convection heat transfer coefficient for CR calculations of T_{mrt}. By directly measuring the h, we eliminate the need for an advanced (and expensive) anemometer and extrapolating correlation that accounts for turbulence intensity beyond their range of validity. Once directly measured, the convective heat transfer can readily be separate from radiation, allowing us to measure T_{mrt} accurately.

The proposed instrument consists of a thin-walled aluminum cylinder with certain external dimensions matching a conventional CR's. The cylinder has two strip heaters attached to its inner wall, and micro-thermocouples epoxied to both inner and outer walls to measure the cylinder surface temperature. To reduce the thermal mass of the device, the center of the cylinder is filled with light plastic foam pieces. This Thesis focuses on the heated cylinder's iterative design, fabrication, and testing. The following Chapters describe the heated cylinder design and fabrication, the construction of the walk-in wind enclosure used for the heated cylinder testing (Chapter 2), and the testing results (Chapter 3). The Thesis is concluded with Chapter 4, which summarizes the performed work and provides suggestions for improvements to the device.

1.8 Summary

This Chapter introduced us to the need for cost-effective, reliable, and accurate ways of measuring radiative heating on the human body. Common methods and nuances of measuring T_{mrt} accurately and cost-effectively were also discussed. Accounting accurately for convection losses in globe and cylindrical radiometers used in outdoor settings that are characterized by high air turbulence were identified as critical to accurate T_{mrt} measurement using these devices. This Thesis addresses this issue by developing a heated cylinder for direct convective losses measurement. Chapter 2 discusses the heated cylinder design and fabrication walk-in wind tunnel testing platform, while Chapter 3 discusses the details of experimental testing of the heated cylinder in the walk-in wind tunnel.

CHAPTER 2

DESIGN AND FABRICATION OF THE HEATER CYLINDER AND ITS TESTING PLATFORM

2.1 Overview of the Heated Cylinder Design and Working Principle

As shown in Figure 2.1a, the heated cylinder consists of an aluminum cylinder with two rectangular heaters and a thermocouple attached to the device's wall. The schematic in Figure 2.1b shows the cylinder's primary heat sources and sinks. Summing these heat fluxes using a steady state surface energy rate balance, we obtain:

$$Q_{heater} + Q_{rad_{abs}} = Q_{conv} + Q_{rad_{em}} + Q_{loss} \tag{2.1}$$

Where $Q_{heater} = IV$ is the power input of the heater (product of input direct current voltage, V, and amperage I), $Q_{rad_{abs}}$ is the sum of short-wave and long-wave absorbed radiation, $Q_{rad_{em}}$ is the emitted radiation, Q_{conv} is the convective heat transfer, and Q_{loss} refers to the heater losses to the environment from the bottom of the cylinder and loss through wire resistances. These quantities can be expressed as:

$$Q_{conv} = A_s h(T_s - T_{air})$$

$$Q_{rad_{abs}} = \alpha_{SW} Q_{SW} + \alpha_{LW} Q_{LW}$$

$$Q_{rad_{em}} = A_s \varepsilon \sigma (T_s + 273)^4 \tag{2.2}$$

Where α_{SW}, α_{LW} are absorbtivities, A_s is the surface area of the cylinder, ε is the emissivity of the cylinder surface, σ is Stefan Boltzmann constant. Knowing the power input into the heater and measuring T_s using the thermocouple, we can calculate the heat transfer coefficient as follows:

$$h = \frac{Q_{heater} + Q_{rad_{abs}} - Q_{rad_{em}} - Q_{loss}}{A_s(T_s - T_{air})}$$

$$A_s = \pi dl \tag{2.3}$$

The radiative gains and losses from the heated cylinder can be minimized by polishing the exterior surface to decrease the absorptivity in both short and long-wave, decreasing the long-wave emissivity. By reducing the radiation terms, convection heat transfer coefficient can be estimated accurately and easily. This instrument was calibrated in the wind enclosure, and the results were benchmarked against the available convection correlations. The tests conducted and analyzed include time to reach a steady state, response time to velocity changes, overall h with varying velocity, the effect of turbulence, and several other minor design aspects that may have a significant effect. The following sub-sections discuss the various iterations of the design and fabrication of the heated cylinder and the wind enclosure setup in which the devices were tested. The conducted experimental results are discussed in the next Chapter.

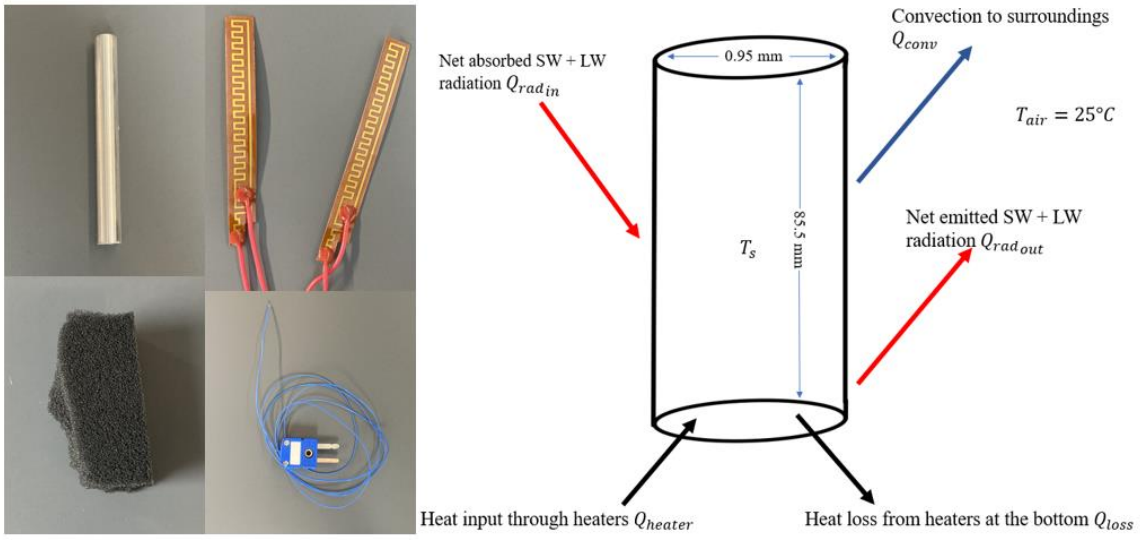

Figure 2.1 (a) Parts of a heated cylinder before assembly and (b) a schematic diagram of the heat fluxes acting on the device.

2.2 The heated cylinder design and fabrication

The goal of this Thesis was to design and fabricate an accurate and fast but cost-effective heated cylinder for measuring the heat transfer coefficient that can be used along with unheated CR to provide accurately T_{mrt} measurement. As summarized above, the working principle is to uniformly heat the cylinder with known power input, measure the resulting outer surface temperature, and use the values to calculate the convection heat transfer coefficient. The device was designed from parts that are widely available with the total prices being less than about $50 (Aluminum cylinder(1ft) ~5$ McMaster-Carr, heaters(4-pack) ~15$ Amazon, thermocouple ~16$ Minnesota Measurement Instruments, epoxy(0.25oz) ~15$ Omega, cost of power supply and acquisition system is not included). The size of the two film heaters (12W flexible Polyimide strip adhesive heaters of 10mm*930mm) was selected so that they could be easily inserted and adhered to the internal walls of the cylinder. Furthermore, the resistance of the heaters was selected so that a typical USB 5V battery could provide a necessary power input (~1 W) for raising surface temperature about 10°C above that of air for an extended period (about the same temperature difference as in standards for thermal manikin measurements [26]). The electrical resistances of the heaters inserted into the cylinder as well as wires connecting to the power source, including soldering points, were measured to account for any power losses outside the cylinder.

The conventional CR design utilizes a thermocouple located at the cylinder's center, which is embedded in epoxy, to ensure its stability and measure its internal temperature [39]. As mentioned in the introduction's CR sub-section, the internal temperature measured may or may not correspond to the cylinder's average surface temperature [39]. To address

this issue, we used one or two micro-thermocouples to measure the internal and external surface temperature of the Aluminum cylinder. The reason for using two thermocouples was to determine whether there were any major temperature differences between the outer and inner surfaces. The thermocouples were secured to the surface using thermally conductive epoxy Omegabond 100 (thermal conductivity of ~1 W/mK). The inside of the cylinder is filled with light expandable foam pieces ($465.58\,kg/m^3$, M-D Building Products), which helps to block the airflow in the cylinder, limiting any convective losses from inside the cylinder. The foam also has a low thermal mass, which reduces equilibration time and causes the input heat to be rejected outwards through the cylinder wall.

We substituted Copper [42] with Aluminum for the cylinder material to minimize the absorbed and emitted radiation. The short wave (extraterrestrial solar) absorptance for smooth (electroplated) Copper is 0.47, while for aluminum foil or polished surface, it is 0.1 or below [40]. Figure 2.2a shows that we fabricated heated cylinders from aluminum tubes with an outer diameter of 0.95 cm (3/8") with wall thicknesses, t, of 1.4 mm and 0.4 mm. To fit only contributing part of the film heaters into the cylinder, we cut the tubes into 8.5 cm tall cylinders (H). Figure 2.2b shows that we also included a top cap for the cylinders to minimize end effects.

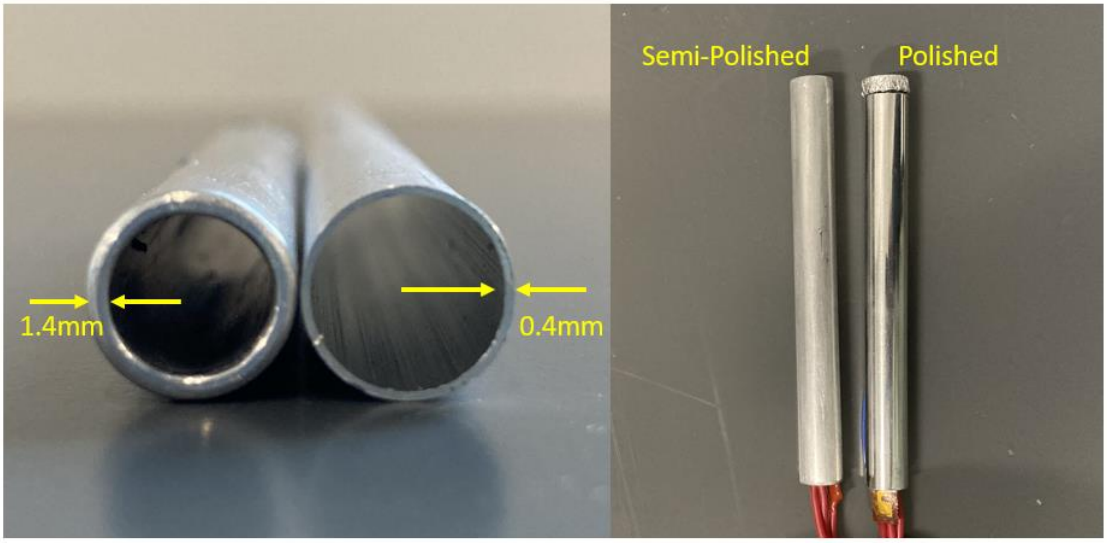

Figure 2.2 (a) Image of the 1.4 mm and 0.4 mm thick Aluminum tubes, and (b) the unpolished heated cylinder along with the polished one with a cap included.

Thermal resistance analysis of the cylinder walls can be used to show that with such dimensions, a minimal temperature change is expected across the cylinder surface. In particular, if the tube wall spreads heat from one side of the cylinder (e.g., exposed to solar flux or with one heater active), the in-plane distance the heat needs to spread on one side is ~0.75 cm. As such, the in-plane thermal resistance ($L/(ktH)$ of the traditional 1 mm thick Copper wall (thermal conductivity, k, of 400 W/mK [41]), the 1.4 mm thick Aluminum wall ($k = 200$ W/mK [41]), and the 0.4 mm thick Aluminum wall are 0.22 K/W, 0.31 W/K, and 1.1 K/W. Assuming that 0.5 W of heat is spread across the 0.75 cm distance of the wall, these thermal resistances would cause a negligible temperature difference of 0.1 K, 0.15 K, and 0.55 K. Even the last temperature difference for the thinner Aluminum wall is with a typical uncertainty of thermocouple measurements.

As purchased, both the thin and thick-walled Aluminum tubes had sufficient surface roughness to have a dull, gray color. To increase the surface's reflectivity, we tried two treatments and measured the resulting spectral reflectivity using a UV-Vis spectrometer and Fourier Transform Infrared Spectroscopy (FTIR) in Arizona State University Core facilities (performed by Dr. Emmanuel Soignard). Specifically, we attempted to hand polish the surface using 1200 grit sandpaper and mechanically polish the surface using Dremel 3000 tool at ~15,000 rpm with Flitz polish compound. The latter procedure was visually judged to yield substantially better results (see an image of the cylinder polished using the Dremel tool in Figure 2.2b).

The reflectivity measurements were done using the DiffusIR module in the Perkin Elmer Frontier FTIR from 400 to 8000 cm^{-1} 16 scans at 0.5cm/s. In turn, the UV-VIS measurement were done using the Perkins Elmer Lambda 950 with a 150 mm spectralon integrating sphere, 2500-800 nm using an InGaAs detector, and 800-250 nm using a PMT detector. Lamp change from tungsten to deuterium at 300 nm—step size 5 nm with the acquisition of 0.52 s/step. The spectral reflectivity for the 0.3 to 2 μm and 2 to 25 μm spectral regions are shown in Figure 2.3. By integrating with the spectral emissive power of the black body at 5800K and 300K, we calculated that the mechanical polishing procedure yielded a short-wave and long-wave hemispherical reflectivity of 0.81 and 0.99. Thus, the procedure yields excellent long-wave reflectivity and minimal absorptivity (i.e., emissivity) but could be improved in the short-wave range.

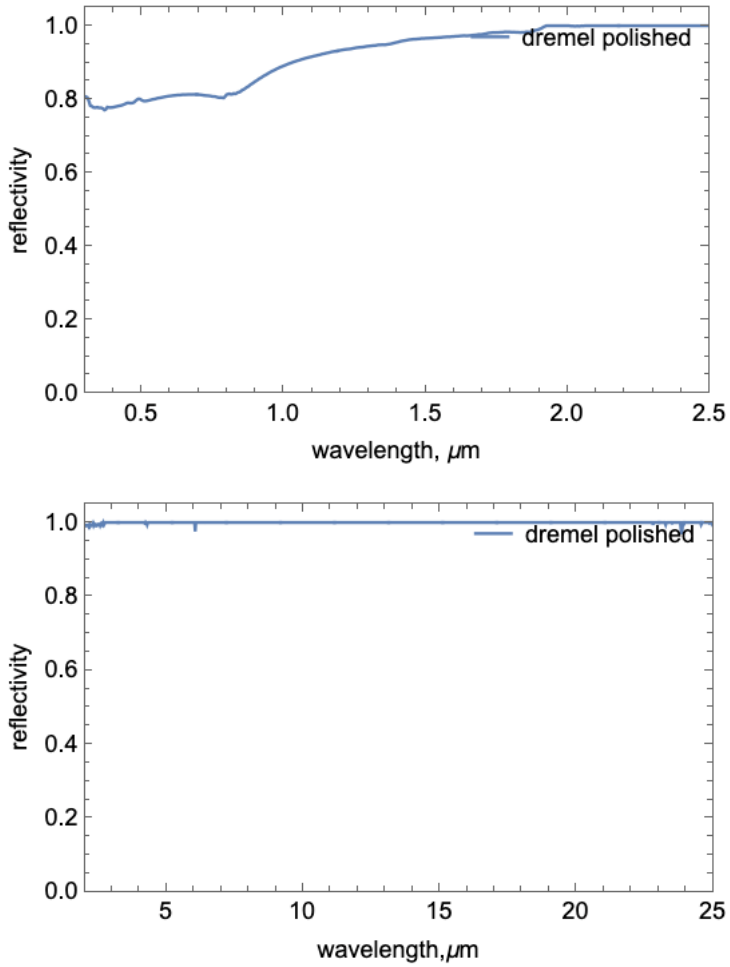

Figure 2.3. The UV-VIS and FTIR reflectivity of the Dremel polished Aluminum.

Throughout the Thesis project, the various design aspects (e.g., thin-walled vs. thick-walled, capped or uncapped heated cylinder, etc.) were iteratively tested using the wind enclosure, and the experimental setup described next. The results of the studies are described in Chapter 3.

2.3 The Wind Enclosure for Heated Cylinder Testing

The heated cylinder was tested using a new walk-in wind enclosure with a continually variable speed of 0.25 to 2 m/s that is located inside a thermal chamber with control temperature and humidity (see Figure 2.4). The thermal chamber is located in Walton Center for Planetary Health on the ASU Tempe campus, inside which the wind enclosure was built by the Thesis author along with several students and Prof. Rykaczewski during the summer of 2022. The sub-sections discuss the experimental conditions, setup, data processing, and error analysis in detail.

2.3.1 The Wind Enclosure and Thermal Chamber

All the experiments were conducted in a controlled environment inside a fully sealed walk-in thermal chamber (BioCold) with temperature and humidity operating ranges of 20°C to 50°C and 10% to 50%, respectively (see Figure 2.4). The temperature and humidity uniformity inside was tested extensively before the present experimental system was set up. For the heated cylinder experiments, the chamber was set to 25°C$\pm$0.5°C and 30% $\pm$ 5% (as per manufacturer) relative humidity for the present tests.

The walk-in wind enclosure is made from 15 mm extruded aluminum framing, supports, and polycarbonate panels (Faztek Industrial Solutions) and was assembled before the start of this study. The enclosure has inner dimensions of 345cm length, 221cm height, 114cm width, and two large side doors for access (see Figure 2.4). All the edges and gaps, if any, were sealed using silicone sealing strips and expandable foam. Gaps cause about a 10 to 20% loss in the velocity inside the chamber and increase turbulence due to flow non-uniformities patterns. The enclosure has a ~6 cm thick honeycomb with 6 mm holes at its

entrance to ensure a laminar air flow and reduce the turbulence intensities to a maximum of about 6%. A set of three 24" fans (Xpower FD-630D) with continual velocity adjustment at the end of the wind tunnel pull in the air through the honeycomb and into the wind tunnel for experimentation. Without any major obstructions, the fans provide nearly uniform airflow in the center of location of the chamber with velocities ranging from 0.25 m/s to 2 m/s.

Figure 2.4, Picture of the thermal chamber with enclosure.

2.4 The Experimental Setup and Procedure

The experiment setup consists of a heated cylinder, a 3D ultrasonic anemometer from Campbell Scientific (CSAT3B) used to measure the air velocity, a 5V power supply

(Tekpower TP3005T) to the strip heaters that are soldered in a series, and a data logging device to log temperature data (Stanford Research Systems, PTC10) from both the thermocouples (Ultra-thin T-type thermocouple AWG36, 0.7mm diameter). The strip heaters have a combined electrical resistance of 28 Ohm, so the voltage was set to 5.25V resulting in 0.191A current and 1 ± 0.05 W power. This power input ensured a minimum temperature difference between the heated cylinder surface and the air surrounding of about 10°C at the maximal velocity of ~2 m/s. Such temperature difference is typically required for human heat transfer coefficient measurements done using thermal manikins [26].

The heated cylinder is vertically mounted onto its stand, as shown in Figure 2.5. The anemometer was placed next to the heated cylinder with the relevant velocity. Care was taken to place them at a reasonable distance to ensure that the anemometer "claws" did not disrupt the flow passing by the heated cylinder. The battery for the anemometer, the heated cylinder power supply, and the data logging system was placed at a lower height behind the heated cylinder and anemometer so as not to cause any disturbances in the flow. The heated cylinder and the anemometer were placed at 1.2 meters height, typically taken for human thermal exposure [32], and in the center of the wind enclosure. Before setting up the experiments, the flow was characterized to ensure we knew the incoming air's accurate velocities and turbulence intensity.

Figure 2.5. Picture of the typical experimental arrangement of the 3D ultrasonic anemometer side-by-side with the heated cylinder.

We recorded the temperatures of the heated cylinder surface at a rate of 8 data points per minute. The heated cylinder's inner and outer surfaces were measured for each time point. The velocity data were collected at a frequency of 25 Hz. Test experiments with an acquisition rate up to 100 Hz were conducted to ensure that 25 Hz was sufficient to capture the velocity fluctuations accurately. The temperature and velocity data for processing were collected for about 5 minutes after reaching the steady state. A steady state was identified based on thermocouple readings when no changes in the readings were observed outside the $\pm$0.5°C fluctuations.

2.5 Data Processing and Error Propagation Analysis

As derived in the sub-section 2.1, knowing the power input into the heater and measuring T_s using the thermocouple, we can calculate the heat transfer coefficient as (repeating equation 2.3):

$$h = \frac{Q_{heater} + Q_{rad_{abs}} - Q_{rad_{em}} - Q_{loss}}{A_s(T_s - T_{air})} \tag{2.4}$$

The Q_{heater} and Q_{loss} are calculated from the total power input (IV) by weighting by the electrical resistance of the heaters inside the cylinder and the wires/connections outside. While the resistances vary slightly from device to device, typical values for the two heater resistances are 27.5 Ohms and the wires/connections 0.5 Ohms. Q_{loss} also accounts for heat loss from the bottom of the cylinder. A small part of the heater (~4% area of heater) is left out of the cylinder, so there is a possible portion of the heat that is not going to the walls of the cylinder. This was estimated on the assumption that the 1 watt of heat is uniformly distributed by the surface of the cylinder, of which 4% is lost to the environment. The $Q_{rad_{em}}$ is calculated using the measured long-wave emissivity of 0.1 (1-reflectivity) and the measured surface temperature. Since the experiments were conducted with lights off, only long-wave surrounding fluxes from the enclosure walls to the cylinder need to be accounted for. Assuming that the enclosure wall temperature is equal to that of the air, $Q_{rad_{abs}} \approx \alpha_{LW} A_s \sigma T_a^4$ where α_{LW} is equal to the long-wave emissivity of the polished surface. Both of these fluxes are on the order of 10^{-3}W, and thus have a minimal impact on the value of the measured heat transfer coefficient.

We calculated the systematic uncertainty of the heat transfer coefficient measurement using the error propagation approach according to the following:

$$U_{h_{sys}} = \sqrt{\left(\frac{\partial h}{\partial Q_{heater}} U_{Q_{heater}}\right)^2 + \left(\frac{\partial h}{\partial Q_{rad}} U_{Q_{rad}}\right)^2 + \left(\frac{\partial h}{\partial Q_{out}} U_{loss}\right)^2 + \left(\frac{\partial h}{\partial A_s} U_{A_s}\right)^2 + \left(\frac{\partial h}{\partial T_s} U_{T_s}\right)^2 + \left(\frac{\partial h}{\partial T_a} U_{T_a}\right)^2} \quad (2.5)$$

Where $U_{h_{sys}}$ is the systematic uncertainty of the h value calculated, $U_{Q_{heater}}, U_{Q_{rad}}, U_{Q_{out}}, U_{A_s}, U_{T_s}, U_{T_a}$ are systematic uncertainties of heaters, due to radiation, heat loss, surface area, surface temperature, and air temperature, respectively. Each of these terms are elaborated below:

$$\frac{\partial h}{\partial Q_{heater}} = \left(\frac{1}{A_s(T_s - T_a)}\right)$$

$$\frac{\partial h}{\partial Q_{rad}} = \left(\frac{-1}{A_s(T_s - T_a)}\right)$$

$$\frac{\partial h}{\partial Q_{out}} = \left(\frac{-1}{A_s(T_s - T_a)}\right)$$

$$\frac{\partial h}{\partial A_s} = \left(\frac{-Q_{heater} + Q_{rad} + Q_{loss}}{A_s^2(T_s - T_a)}\right)$$

$$\frac{\partial h}{\partial T_s} = \left(\frac{-Q_{heater} + Q_{rad} + Q_{loss}}{A_s(T_s - T_a)^2}\right)$$

$$\frac{\partial h}{\partial T_a} = \left(\frac{-Q_{heater}+Q_{rad}+Q_{loss}}{A_s(T_s-T_a)^2}\right) \quad (2.6)$$

The values of $U_{Q_{rad}}$, $U_{Q_{loss}}$ and U_{A_s} was estimated in a similar fashion respectively before including them for estimating the uncertainty in h. The T_s , T_a and Q_{heater} are sensitivities from the measuring instruments available from the manufacturer.

Each experiment was repeated three (or more) times, and the random error contribution (statistical) was calculated using T-student distribution with a confidence interval of 80% are reported (i.e., $\pm$1.886 standard deviations). The random (from repeated measurements) and systematic (from instruments) errors were combined to yield total uncertainty according to the:

$$U_{h_{total}} = \sqrt{U_{h_{random}}^2 + U_{h_{sys}}^2} \quad (2.7)$$

2.6 Summary

This Chapter discusses about the design, fabrication, and testing of the heated cylinder to measure the convective heat transfer coefficient directly to account for it in the measurement of T_{mrt}. The iterative design approaches and fabrication were discussed in detail, along with the experimental setup and environmental conditions covered above. In the next Chapter, the tests conducted and analyzed are discussed, which include time to reach a steady state, response time to velocity changes, overall heat transfer coefficient with varying velocity, and other minor design changes that may have a significant effect. These will be discussed in detail in the result and discussion section.

CHAPTER 3

TESTING OF THE HEATED CYLINDER

3.1 Overview of Tests Conducted

A constant room temperature of 25°C±1°C and 30% relative humidity were maintained for the current tests. The heaters were given an input of 1 W, which then heated the surface of the cylinder. We need to consider several factors that can significantly affect the system's performance. These include the time required for the system to achieve a steady state, how quickly the system can respond to changes in velocity, the convective heat transfer coefficient under varying velocities, and any design changes that can have a significant impact on the required results. Multiple tests were conducted to understand these factors, which are discussed in detail in the following sub-sections.

3.2 Time to Reach Steady State

The first set of tests were conducted to understand the time taken for the heated cylinder to reach a steady state once the heating was turned on. The cylinders were heated with 1 W while the wind tunnel maintained a constant air velocity of 1 m/s. The data from the thermocouple was collected at 0.12 Hz until temperature fluctuations were under 0.25 °C. Both the heated cylinders with 1.4mm and 0.4mm wall thickness were tested to determine the impact of wall thickness on equilibration time.

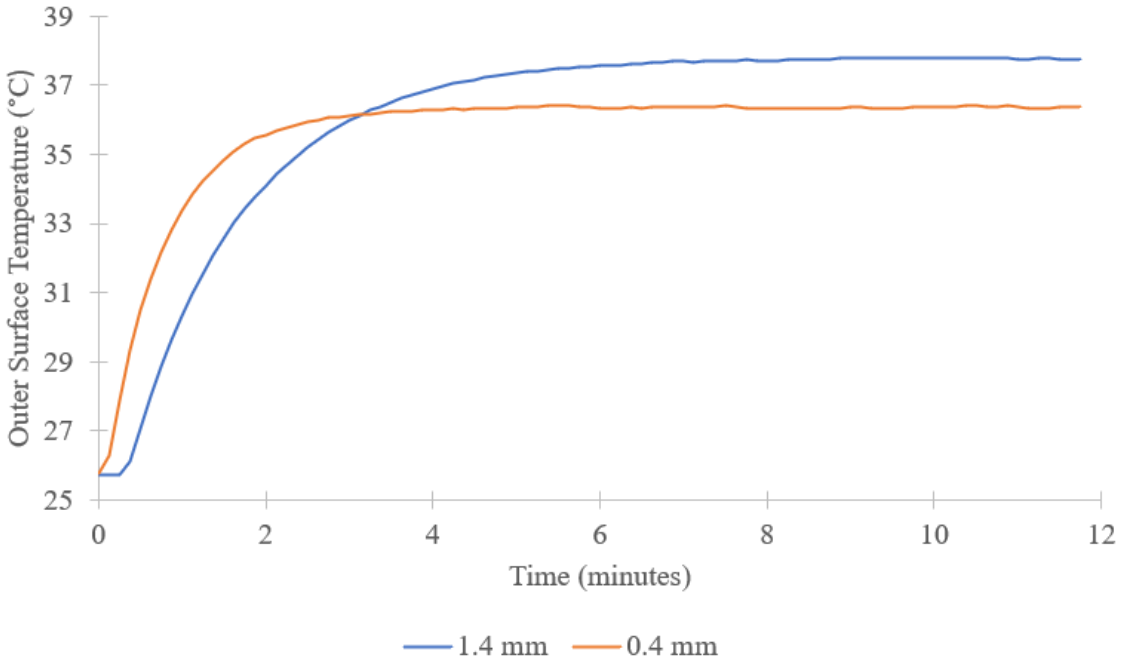

Figure 3.1. Time taken for the heated cylinders to reach a steady state.

The plot in Figure 3.1 shows the time taken for both thicknessed cylinders to reach a steady surface temperature. It can be seen that 1.4mm thick cylinder takes about 7 minutes to reach a constant surface temperature while the 0.4mm thick cylinder takes only about 3 minutes, a more than 50% reduction in time. This is a much shorter time as compared to a standard globe thermometer, which takes about 20 minutes to reach a steady state [23] or even ping-pong ball versions that take about 5 minutes[25] . The shorter time required to reach a steady state is important outdoors, where the environment can change rapidly.

The large difference in time required to reach a steady state for the two cylinder thicknesses is due to their thermal mass (product of specific heats with their mass). Owing to the faster equilibration, the 0.4 mm thick cylinders are a better choice in this case as compared to the 1.4 mm thick cylinder. Therefore, from here on, all the tests were conducted only on 0.4 mm thick cylinders.

Another point to note here is that these times are for a cylinder at room temperature and heated while keeping the velocity of incoming air constant. In practice, during outdoor conditions, what might be more relevant is the cylinder response to a sudden change in air velocity. Such step change response is evaluated in the following sub-section.

3.3 Heated Cylinder Response to Step Change in Air Velocity

Air velocity step change tests was performed to understand how long it takes for the heated cylinder to respond when there is a sudden (step) change in the velocity of the incoming air. Specifically, the response of a heated cylinder after it reached equilibrium temperature to an abrupt air velocity change was measured.

For the first case, the cylinder was heated in the presence of 1.5 m/s constant velocity. Once it reached a steady state (a constant temperature of ~35°C), the velocity was manually changed to 0.5 m/s, and temperature data was collected until after it adjusted and reached a constant temperature of ~39°C. The second case followed the same procedure, but the velocity was changed from 0.5 m/s to 1 m/s. The thermal chamber was maintained at 25°C and 30% humidity throughout these tests.

The variation of temperature in response to abrupt velocity changes can be observed in Figure 3.2. It can be observed that, for both step sizes, it takes about ~2.5 minutes for the heated cylinder to adjust to the velocity change and reach a steady state. This time period is close to the time it takes for the heated cylinder at room temperature to reach equilibrium when exposed to 1 m/s airflow. Now that we established that the heated cylinder responds quickly to the changes in its surroundings let us look at the variation of convection heat transfer coefficient with the air velocity.

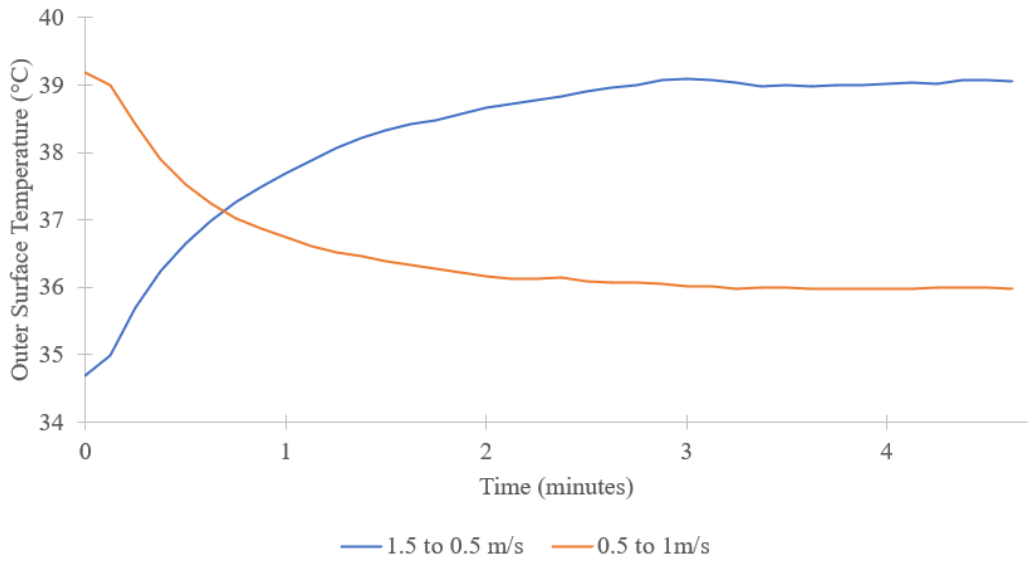

Figure 3.2. Time taken for the heated cylinders to reach a steady state when exposed to a sudden change in air velocity.

3.4 Effect of Velocity Variation on Convective Heat Transfer Coefficient Value

These tests aimed to understand the accuracy of the heated cylinder for measuring the convection heat transfer coefficient as velocity varies. At a constant heat input to the walls, the velocity was varied as in step sizes of 0.5 m/s giving us data at four different velocities, 0.5, 1, 1.5, and 2 m/s, while maintaining the air temperature and humidity at 25℃ and 30% humidity. The convection heat transfer coefficient (h) was calculated based on the outer surface thermocouple readings (discussed in chapter 2) collected for about 5 minutes after reaching the steady state.

3.4.1 Quantifying Edge Effects: Comparison of Uncapped and Capped Heated Cylinder

A comparison was made for polished cylinders ($\varepsilon = 0.01$) without cap and with cap; see Figure 3.3. It can be expected that when there is no proper way to seal the top of the

cylinder, there will be heat loss through the opening rather than heat loss through the walls. To seal the top end of the cylinder, we used an acrylic panel cut in the diameter of the cylinder and covered with Aluminum foil to make it reflective. Figure 3.3, shows clear distinction that the h value for the uncapped cylinder is less than that for the capped cylinder. This outlines that the heat loss through the ends of the cylinder, if not appropriately sealed, affects the overall convection heat transfer coefficient by about 14%, which is a significant number for a cylinder this scale. In the next subsection, let us compare the h value of a capped heated cylinder with existing classic correlations using velocity data.

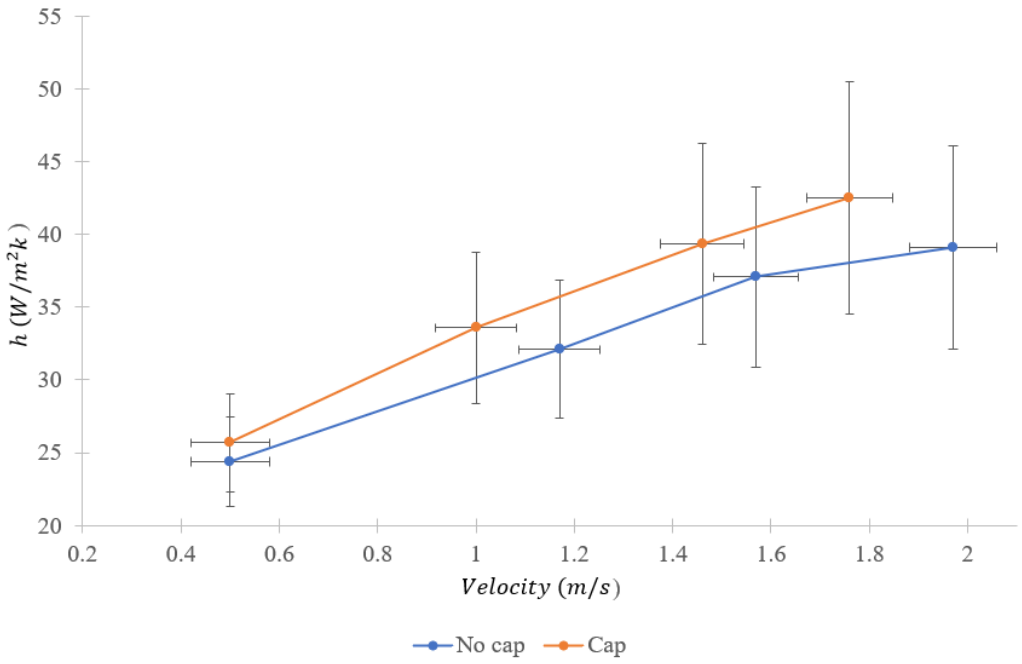

Figure 3.3. Comparison of measured convective heat transfer coefficient (h) for heated cylinders without a top cap and with a top cap.

3.4.2 Comparison of inner and outer surface temperature

The h value should be calculated using the outer surface temperature. Since the Aluminum wall is essentially isothermal across its thickness, the temperature can be

measured on the inner or outer surface. Figure 3.6. compares the measured inner and outer surface temperatures at different air velocities.

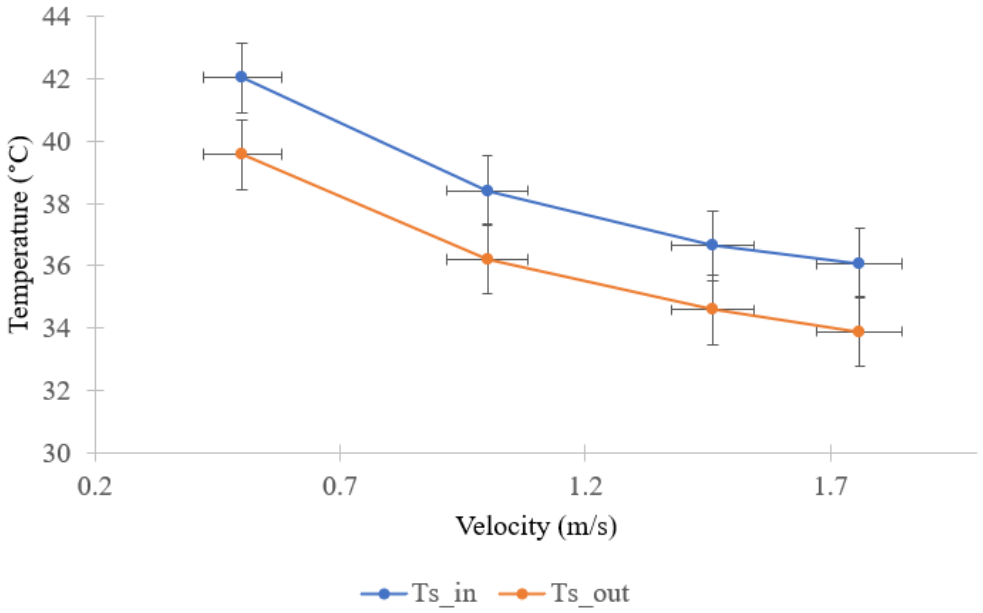

Figure 3.4. Comparison of inner and outer surface temperatures of the heated cylinder.

The plot in Figure 3.4 shows that the inner thermocouple reading is about 2°C higher than the outer one. Most likely, this difference stems from the exposure of the outer thermocouple to moving air and the proximity of the inner thermocouple to the wall-glued heaters. Another potential reason for the temperature difference can be the thermal resistance of the wall as well as the epoxy thermocouple mounting. Naturally, basing the h calculation on the temperature ($T_{s_{in}}$ or $T_{s_{out}}$) will impact the results, which we discuss next.

Figure 3.5 compares the h value calculated using Equation 2.4 employing either the inner or outer surface temperatures. Using the inner surface temperature gives a convection coefficient value of about 5 W/m2K lower than the outer surface temperature. Such a trend

can be expected because the higher the surface temperature, the lower the heat transfer coefficient. The next section compares the measured h values against classic correlations from chapter 1.

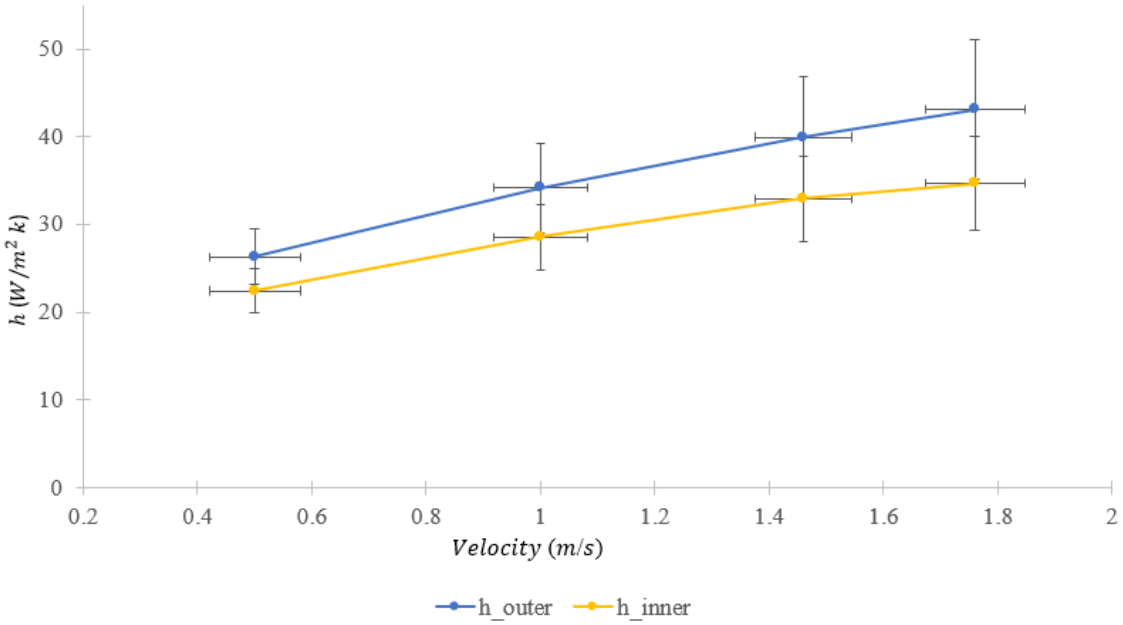

Figure 3.5. Comparison of h calculated using outer and inner surface temperatures.

3.4.3 Comparison of h Value from Heated Cylinder and Correlations

This Section compares the calculated h values based on the inner and the outer surface thermocouple readings against predictions of classical correlations for cylinders in a crossflow. The plot in Figure 3.4 shows that the calculated h values based on thermocouple data fall in between the two correlations considered (within 13% of it). The small deviation of the measured and predicted values likely stems from the ~5% turbulence intensity present in the air, which is not explicitly accounted for in the correlations, but is known to have a significant effect on h as per Figure 1.3 in chapter 1.

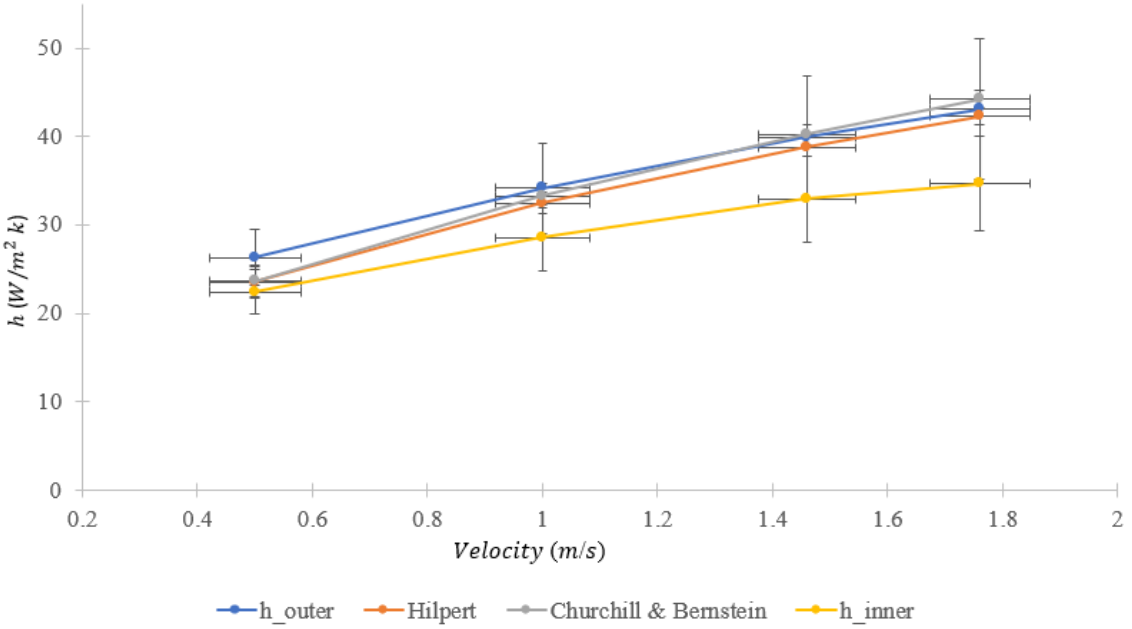

Figure 3.6. Comparison of calculated h with classical correlations for estimating h for a cylinder in crossflow.

But as discussed in chapter 1, the legacy CRs and Globe Thermometers use thermocouple placed at the center of the device, and it is assumed that the center temperature is equal to the surface temperature. But, from section 3.4.2, the h value from the inner surface temperature value is considerably lower than the h value using the outer surface temperature value. It can thus be said that using the inner surface temperature or center temperature underestimates the h value in our case. This is also expected to persist in the case of existing CR and Globe Thermometers since they assume the center temperature to be equal to outer surface temperature[20].

3.5 Summary

This chapter discusses the experiments conducted to understand the functioning of the heated cylinder and to see if the convective heat transfer coefficient, h, directly

estimated agrees with the h value calculated using classic correlations. Each section in the chapter deals with different aspects of heated cylinder properties, from the time taken for the heated cylinder to reach equilibrium to calculating h value. It was demonstrated that the thinner heated cylinder reaches equilibrium about 50% quicker than the thicker one. The h value, calculated directly based on surface temperature, matches well in range with the correlations for a cylinder in cross flow. This Thesis is concluded by summarizing the work done so far and discussing possible future work in the next chapter.

CHAPTER 4

CONCLUSION AND FUTURE WORK

4.1 Discussion

So far, when accounting for convection while estimating T_{mrt}, convection correlations were used to estimate the h value[20], [42]. This process usually involves collecting the air velocity data and calculating the Reynolds number to estimate the Nusselt number and, in turn, h value, which is used to account for convection. As discussed in the introduction chapter, accurately accounting for convection is very important for the precise estimation of T_{mrt}. However, this above-discussed process is relatively complex and does not account for turbulence present in the air (see section 1.7). The correlations commonly used for cylinders are Hilpert [30] and Churchill and Bernstein [31]. These correlations were developed in indoor wind tunnels with minimal or no free-stream turbulence, so we do not know how they will hold true in the presence of TI.

Many studies include TI and proposed their own correlations, which seem to be valid only for a particular Re and TI range. For example, Sak et al. [38] proposed a correlation for horizontal heated cylinders under cross flow for low TI (3% to 8.2%). Lowery and Vachon [34] proposed another correlation that is valid for much higher Re ranges ~ 10^6. Konjoyan and Daudin [33] studied both circular and elliptical cylinders. While the studies mentioned above experimentally determined the correlations, Ahn et al. [36] improved them using numerical simulations. However, even after all the work done so far in this field, the correlations are very specific to a certain range and cannot be applied universally. No correlation between TI and Nu or h is available for the range of TI and Re we observed in our experiments. Furthermore, measuring turbulence requires fast 3D

anemometers that can collect velocity measurements in 3 directions at high frequencies, which can be used to estimate the TI value. This makes the entire process even more complicated and expensive.

Due to the rise in global temperatures and with radiant heat playing a major role in heating the human body exposed to these extreme temperatures, we need methods that can easily and accurately estimate T_{mrt}, especially for accounting convection. A possible way to reduce costs while not compromising the accuracy of convection correction would be to measure the convection heat transfer coefficient (h) directly, avoiding the need to measure TI. We proposed using an Aluminum heated cylinder to directly measure this h value instead of using the correlations mentioned above.

The surface temperatures measured on the heated cylinder, along with heat input through heaters, can be used to directly calculate the convection heat transfer coefficient, h. Since the thermal environment is a combination of radiation and convection, to accurately calculate h value, we need to minimize the thermal radiation. This is why highly reflective ($\varepsilon = 0.01$) metal like Aluminum was chosen. This concept of coating or directly using less emissive materials to reduce radiation heat fluxes has been performed previously for various purposes [43]–[46]. By incorporating this idea into the heated cylinder, we were able to minimize net thermal radiation to as low as $0.001\ W$ range in the long-wave region (No solar load). When exposed to direct solar load we can expect this to go as high as 0.5W.

The heated cylinder proposed in this Thesis can be deployed along with conventional CR to estimate T_{mrt}. This can potentially eliminate the need to use 3D anemometers for getting velocity and TI data for accounting for convection. Once fully

tested and developed, the entire T_{mrt} estimation system will require only a conventional CR (for calculating absorbed radiation) and a heated cylinder (for calculating h value).

A sample set of data was taken from Vanos et al.[20] for tan cylindrical radiometer exposed to solar thermal load. The samples were taken such that their air velocity matched with air velocities in our experiments. The T_{mrt} was estimated using Equation 1.9, discussed in the introduction chapter. Potential error in T_{mrt} due to an error in h was also estimated, but the error bars are minimal since the possible error is small. This small error in T_{mrt} is possible because it is dependent on h only under the fourth root. We can see the variation of errors in T_{mrt} with variation in h error in Figure 4.2. This T_{mrt} error propagation analysis follows like Equation 2.5 using partial derivatives, considering only the h error. The possible errors from the sample data of CR were neglected for simplicity. However, it is still required to test this setup (both CR and heated cylinder together) under direct solar load to better estimate and understand the results.

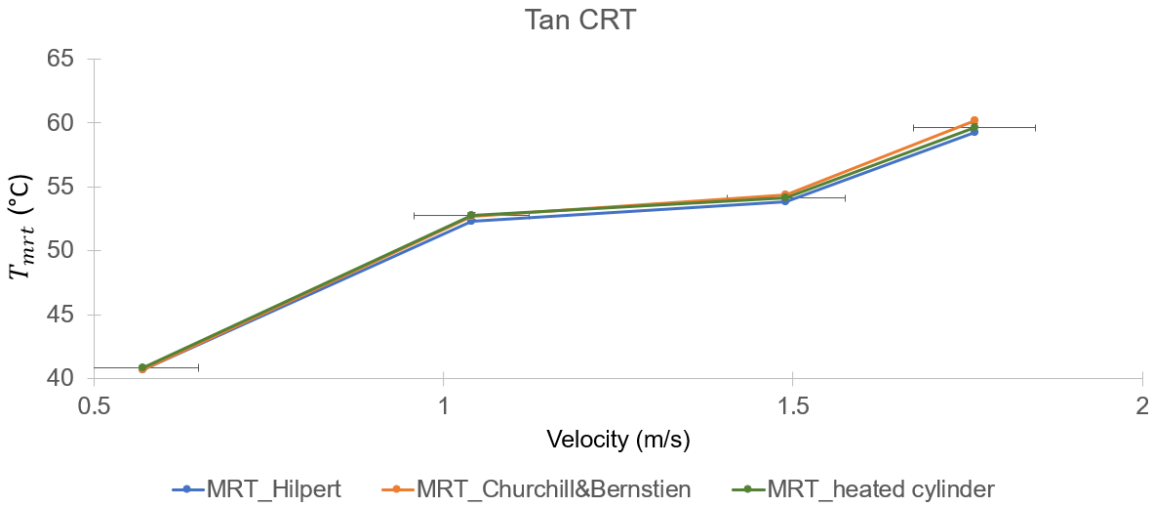

Figure 4.1. T_{mrt} estimation using heated cylinder and comparison with correlations for a sample data from Vanos et al.[20].

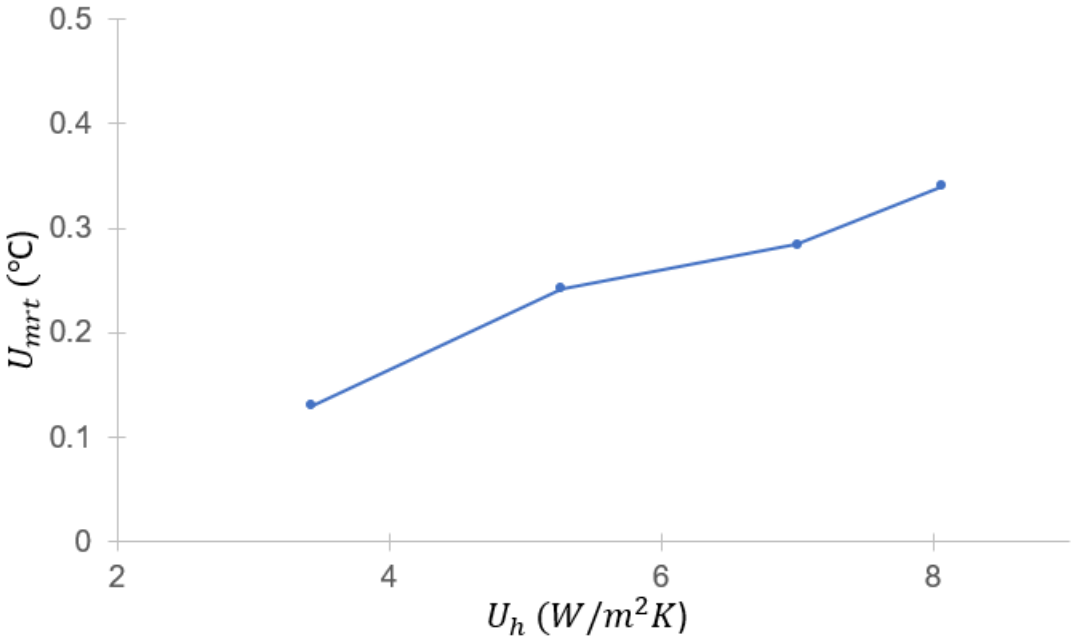

Figure 4.2. T_{mrt} error variation with h error.

4.2 Conclusion

The goal of the present study was to develop a device for directly measuring the convection heat transfer coefficient (h) and account for it in measuring T_{mrt}. A small, heated cylinder was iteratively designed, fabricated, and tested to achieve this. The main design is discussed in Chapter 2, along with the environmental setup for the testing conditions. All the parts used to make the heated cylinder together cost around $50, making it cost-effective yet reliable as compared to other modes of measuring h for accounting convection in estimating T_{mrt}. Various tests were conducted to evaluate the device's performance, which was discussed in Chapter 3. The 0.4 mm thick heated cylinder with a cap has reached a steady state in about 2.5 minutes and provides heat transfer coefficient values that agree with classical correlations within 13%, showing proof of concept.

4.3 Future work

The primary recommended improvement focuses on measuring the cylinder's exact shell or wall temperature. Instead of epoxying the thermocouple directly to the wall, a small grove for the thermocouple head as well as its wire, can be made on the surface of the cylinder (see Figure 4.2). To completely cover even this small, exposed area and make it uniform, Aluminum tape can be used. The thermocouple can be passed through the inside of the cylinder through a small hole near the attachment point.

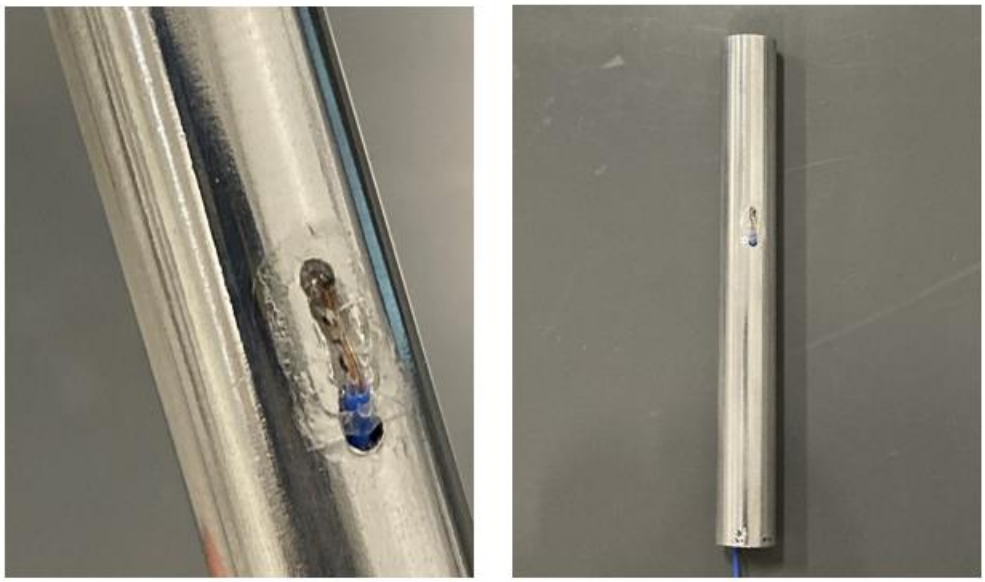

Figure 4.3. Improved heated cylinder design with a hole and grove for thermocouple.

Along with this, we also recommend experimentally testing the uniformity of the shell temperature along the circumference of the cylinder (Azimuth angle). We initially tried taking a thermal image to show this uniformity. However, due to the reflective nature of Aluminum, its response to an IR camera varies even when the entire surface is at a similar temperature—making it look as if the temperature across the surface is not very uniform. This is because the IR camera detects the thermal energy or heat emitted. We also

noticed that the spectral properties of epoxy vary, making it look like it is at a very high temperature even when it is not. To overcome this, we used a 2cm, single-layer blue painters' tape, affixed it along the cylinder, and retook the thermal images. This can be observed in Figure 4.4, and the area with tape can be seen as a bright uniform band, proving that the surface temperature is indeed uniform. However, we would recommend experimentally testing it by collecting surface temperature data at different Azimuth angles (i.e., by rotating the heated cylinder) at a certain velocity and comparing if they are the same.

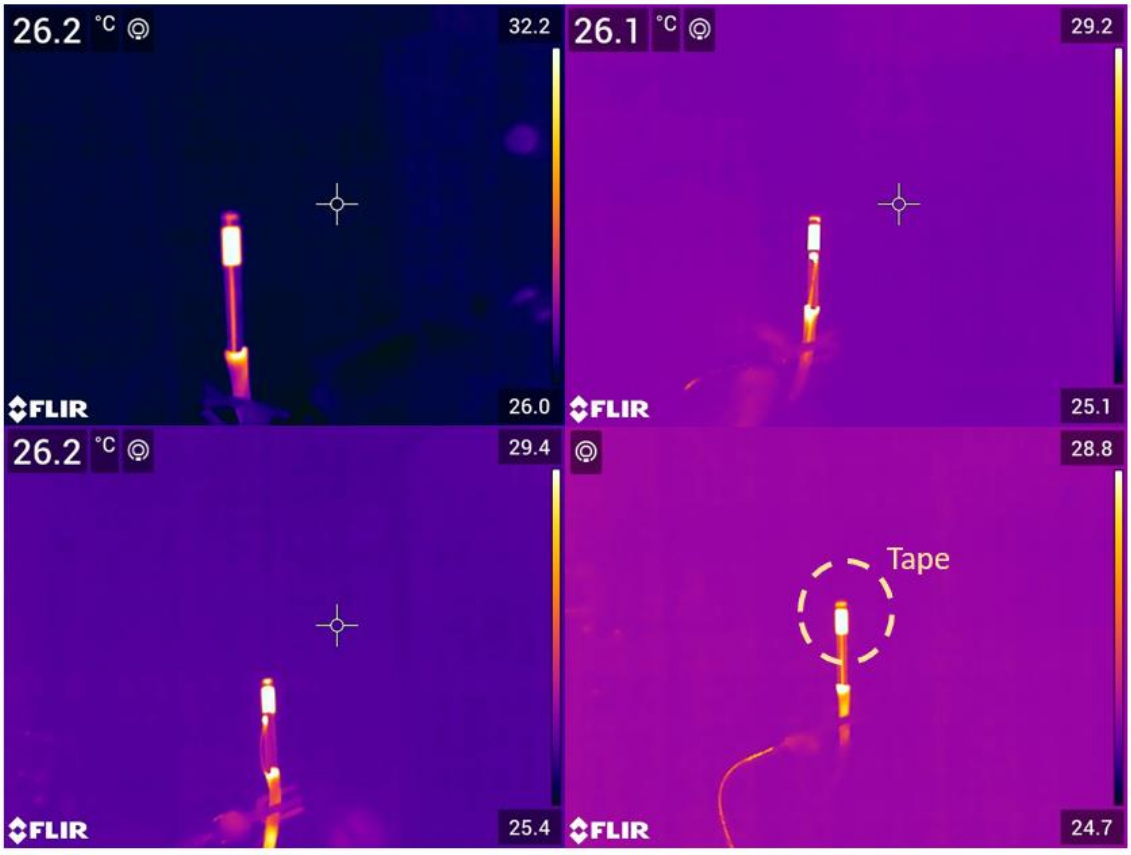

Figure 4.4. Thermal images of the heated cylinder with tape exposed to 1m/s velocity of air.

Another major step is to validate the heated cylinder outdoors when exposed to a direct solar load. On top of that, we need a better way to include turbulence intensity in benchmarking the calculated h value for greater accuracy and understanding. Then using this method to estimate T_{mrt} and validate it against other methods of measuring it to see the effectiveness of the proposed method. It will also be interesting to see how cylinders of different lengths and diameters will respond to the same conditions and pick one that will be the closest to existing standard devices.

REFERENCES

[1] U. N. DESA, "United Nations Department of Economic and Social Affairs/Population Division: World Population Prospects: The 2008 Revision. 2009b," *Reference Source*, 2021.

[2] A. Middel and E. S. Krayenhoff, "Micrometeorological determinants of pedestrian thermal exposure during record-breaking heat in Tempe, Arizona: Introducing the MaRTy observational platform," *Science of the Total Environment*, vol. 687, pp. 137–151, Oct. 2019, doi: 10.1016/j.scitotenv.2019.06.085.

[3] S. W. Kim and R. D. Brown, "Urban heat island (UHI) intensity and magnitude estimations: A systematic literature review," *Science of the Total Environment*, vol. 779. Elsevier B.V., Jul. 20, 2021. doi: 10.1016/j.scitotenv.2021.146389.

[4] P. Rajagopal, R. S. Priya, and R. Senthil, "A review of recent developments in the impact of environmental measures on urban heat island," *Sustainable Cities and Society*, vol. 88. Elsevier Ltd, Jan. 01, 2023. doi: 10.1016/j.scs.2022.104279.

[5] C. Mora *et al.*, "Global risk of deadly heat," *Nat Clim Chang*, vol. 7, pp. 501–506, 2017.

[6] K Parsons, *Human thermal environments: the effects of hot, moderate, and cold environments on human health, comfort, and performance*. 2014.

[7] C. Mora, C. W. W. Counsell, C. R. Bielecki, and L. V Louis, "Twenty-seven ways a heat wave can kill you: deadly heat in the era of climate change," *Circ Cardiovasc Qual Outcomes*, vol. 10, no. 11, p. e004233, 2017.

[8] K. L. Ebi *et al.*, "Hot weather and heat extremes: health risks," *The lancet*, vol. 398, no. 10301, pp. 698–708, 2021.

[9] P. O. Fanger, *Thermal comfort: analysis and applications in environmental engineering, by P. O. Fanger.* New York: McGraw-Hill, 1972.

[10] A. Yoshida, T. Naka, N. Chigusa, and S. Kinoshita, "Thermal sensation and thermal load of human body in irradiated hot environment," *Urban Clim*, vol. 36, Mar. 2021, doi: 10.1016/j.uclim.2020.100765.

[11] F. Meggers *et al.*, "The Thermoheliodome–'Air conditioning' without conditioning the air, using radiant cooling and indirect evaporation," *Energy Build*, vol. 157, pp. 11–19, 2017.

[12] N. Kántor and J. Unger, "The most problematic variable in the course of human-biometeorological comfort assessment—the mean radiant temperature," *Central European Journal of Geosciences*, vol. 3, pp. 90–100, 2011.

[13] A. Joshi, A. Psikuta, M.-A. Bueno, S. Annaheim, and R. M. Rossi, "Analytical clothing model for sensible heat transfer considering spatial heterogeneity," *International Journal of Thermal Sciences*, vol. 145, p. 105949, 2019.

[14] H. Guo, D. Aviv, M. Loyola, E. Teitelbaum, N. Houchois, and F. Meggers, "On the understanding of the mean radiant temperature within both the indoor and outdoor environment, a critical review," *Renewable and Sustainable Energy Reviews*, vol. 117. Elsevier Ltd, Jan. 01, 2020. doi: 10.1016/j.rser.2019.06.014.

[15] H. Arthur, "Barker, radiant heating," *Proceedings of the Institution of Heating and Ventilating Engineers*, vol. 25, p. 141, 1926, [Online]. Available: https://www.scopus.com/inward/record.uri?eid=2-s2.0-85074744042&partnerID=40&md5=47e22bc2a7b1f46991958a592fa2aa1d

[16] P. S. B. Newling, "The measurement of mean radiant temperature and the determination of the amount of radiant heat gained by a man," *Med. Res. Coun., Lond., RNP Rep*, no. 54/784, 1954.

[17] R. D. Brown, "Correcting the error in measuring radiation received by a person: introducing cylindrical radiometers," *Sensors*, vol. 19, no. 23, p. 5085, 2019.

[18] K. Rykaczewski, L. Bartels, D. M. Martinez, and S. H. Viswanathan, "Human body radiation area factors for diverse adult population," *Int J Biometeorol*, vol. 66, no. 11, pp. 2357–2367, 2022.

[19] K. Rykaczewski, J. K. Vanos, and A. Middel, "Anisotropic radiation source models for computational thermal manikin simulations based on common radiation field measurements," *Build Environ*, vol. 208, p. 108636, 2022.

[20] J. K. Vanos, K. Rykaczewski, A. Middel, D. J. Vecellio, R. D. Brown, and T. J. Gillespie, "Improved methods for estimating mean radiant temperature in hot and sunny outdoor settings," *Int J Biometeorol*, vol. 65, no. 6, pp. 967–983, Jun. 2021, doi: 10.1007/s00484-021-02131-y.

[21] B. T. Bedford and C. G. Warner, "THE GLOBE THERMOMETER IN STUDIES OF HEATING AND VENTILATION."

[22] H. M. Vernon, "The measurement of radiant heat in relation to human comfort.," *Journal of Industrial Hygiene*, vol. 14, pp. 95–111, 1932.

[23] D. A. McIntyre, *Indoor climate*. Elsevier, 1980.

[24] R. de Dear, “PING-PONG GLOBE THERMOMETERS FOR MEAN RADIANT TEMPERATURES.,” *H and V Engineer*, vol. 60, no. 681, pp. 10–11, 1987.

[25] S. Thorsson, F. Lindberg, I. Eliasson, and B. Holmer, “Different methods for estimating the mean radiant temperature in an outdoor urban setting,” in *International Journal of Climatology*, Nov. 2007, pp. 1983–1993. doi: 10.1002/joc.1537.

[26] K. Parsons, *Human thermal environments: the effects of hot, moderate, and cold environments on human health, comfort, and performance*. CRC press, 2014.

[27] R. D. Brown, “Correcting the Error in Measuring Radiation Received by a Person: Introducing Cylindrical Radiometers,” *Sensors*, vol. 19, no. 23, p. 5085, 2019.

[28] S. A. Krys and R. D. Brown, “I |L 17 R@ meteorology Radiation absorbed by a vertical cylinder in complex outdoor environments under clear sky conditions,” 1990.

[29] R. D. Brown and T. J. Gillespie, “Estimating Outdoor Thermal Comfort Using a Cylindrical Radiation Thermometer and an Energy Budget Model,” 1986.

[30] R. Hilpert, “Heat transfer from cylinders,” *Forsch. Geb. Ingenieurwes*, vol. 4, no. 5, p. 215, 1933.

[31] S. W. Churchill and M. Bernstein, “A correlating equation for forced convection from gases and liquids to a circular cylinder in crossflow,” 1977.

[32] J. Zou, Y. Yu, J. Liu, J. Niu, K. Chauhan, and C. Lei, “Field measurement of the urban pedestrian level wind turbulence,” *Build Environ*, vol. 194, p. 107713, 2021.

[33] A. Kondjoyan and J. D. Daudin, “Effects of free stream turbulence intensity on heat and mass transfers at the surface of a circular cylinder and an elliptical cylinder, axis ratio 4,” 1995.

[34] G. W. Lowery and R. I. Vachon~, “THE EFFECT OF TURBULENCE ON HEAT TRANSFER FROM HEATED CYLINDERS,” Pergamon Press, 1975.

[35] S. D. Sikmanovic, S. N. Oka, and S. Koncar-Djurdjevic, “Influence of the structure of turbulent flow on heat transfer from a single cylinder in a cross flow,” in *International Heat Transfer Conference Digital Library*, Begel House Inc., 1974.

[36] J. Ahn, E. M. Sparrow, and J. M. Gorman, “Turbulence intensity effects on heat transfer and fluid-flow for a circular cylinder in crossflow,” *Int J Heat Mass Transf*, vol. 113, pp. 613–621, 2017, doi: 10.1016/j.ijheatmasstransfer.2017.05.131.

[37] A. B. Mehendale, J. C. Han, and S. Ou, “Influence of high mainstream turbulence on leading edge heat transfer,” 1991.

[38] C. Sak, R. Liu, D. S. K. Ting, and G. W. Rankin, “The role of turbulence length scale and turbulence intensity on forced convection from a heated horizontal circular cylinder,” *Exp Therm Fluid Sci*, vol. 31, no. 4, pp. 279–289, Feb. 2007, doi: 10.1016/j.expthermflusci.2006.04.007.

[39] J. K. Vanos, K. Rykaczewski, A. Middel, D. J. Vecellio, R. D. Brown, and T. J. Gillespie, “Improved methods for estimating mean radiant temperature in hot and sunny outdoor settings,” *Int J Biometeorol*, vol. 65, no. 6, pp. 967–983, 2021.

[40] M. F. Modest, *Radiative heat transfer*. San Diego: Academic press, 2013.

[41] T. L. Bergman, A. S. Lavine, F. P. Incropera, and D. P. Dewitt, *Fundamentals of heat and mass transfer*. New York: John Wiley & Sons, Inc, 2011.

[42] E. Teitelbaum *et al.*, “Globe thermometer free convection error potentials,” *Sci Rep*, vol. 10, no. 1, Dec. 2020, doi: 10.1038/s41598-020-59441-1.

[43] R. J. De Dear, E. Arens, Z. Hui, and M. Oguro, “Convective and radiative heat transfer coefficients for individual human body segments,” *Int J Biometeorol*, vol. 40, pp. 141–156, 1997.

[44] U. Danielsson, “Convection coefficients in clothing air layers.,” 1996.

[45] D. Quintela, A. Gaspar, and C. Borges, “Analysis of sensible heat exchanges from a thermal manikin,” *Eur J Appl Physiol*, vol. 92, pp. 663–668, 2004.

[46] M. Fojtlín, J. Fišer, and M. Jícha, “Determination of convective and radiative heat transfer coefficients using 34-zones thermal manikin: Uncertainty and reproducibility evaluation,” *Exp Therm Fluid Sci*, vol. 77, pp. 257–264, Oct. 2016, doi: 10.1016/j.expthermflusci.2016.04.015.